Wind-Tolerant Event-Based Adaptive Sliding-Mode Control for VTOL Rotorcrafts Multi-Agent Systems

Jonatan Alvarez-Munoz, Juan-Antonio Escareno, J. Chevalier, S. Daix, Ouiddad Labbani-Igbida

Wind-Tolerant Event-Based Adaptive Sliding-Mode Control for VTOL Rotorcrafts Multi-Agent Systems

J. U. Alvarez-Muñoz[1,*], J. Escareno[2], J. Chevalier[1], S. Daix[3], O. Labanni-Igbida[2]

***Abstract*—The present paper investigates the consensus control of a Multi-Agent System (MAS) composed by Vertical Take-off and Landing (VTOL) rotorcrafts subject to aerodynamic disturbances. Initially, the attitude's VTOLs model based on quaternion formalism is detailed to subsequently derive the corresponding control law. Likewise, the MAS translational dynamics is extended to entail the airframe's aerodynamics. In order to achieve the consensus objective, a robust adaptive event-triggered sliding-mode control (SMC) is synthesized considering a leader-follower scheme guaranteeing Lyapunov's closed-loop stability and avoiding the Zeno behavior. Results from an extensive simulation stage witness the effectiveness of the proposed control scheme. The latter allows to fulfill the collective consensus and leader's trajectory tracking objectives in presence of unknown disturbances while keeping a reduced computational cost.**

I. Introduction

Recently, achievable missions of Unmanned Aerial Vehicles (UAV) multi-agent systems (MAS) within the civilian and industrial sectors have motivated the scientific community to increase its research efforts. Current MAS-based applications like precision agriculture, environmental monitoring or cargo transportation, just to mention a few, require energy efficient onboard control modules to enhance flight endurance while exhibiting robustness against adverse atmospheric conditions.

Compared to continuous-time control techniques, which can be deteriorated due to limited communication bandwidth, the event-based control methodologies manage and reduce the usage of the network bandwidth and computing resources. Essentially, the event-based control computes and updates the control signals when specific conditions are met, i.e. an event occurs. Thus, for multi-agent systems based on such control scheme, the information exchange among agents is no longer periodical and it occurs only when necessary. On this subject, the study of single and double integrator agents show the relevance of event-based controllers when featuring communication delays, packet drops or noise [1], [2], [3], [4].

Other important issues of multi-agent systems include the presence of disturbances or model uncertainties. In this regard, different works have considered adaptive and robust control techniques combined with event-triggered mechanisms, as in [5], [6] and [7]. Among the robust control techniques, the sliding mode control strategy is well known for its robustness face to time-varying disturbances, as it is shown in [8]. For example, in [9], an integral sliding mode controller is combined with an event-triggered mechanism for the consensus problem of second order multi-agent systems. [10] deals with the leader-following consensus problem of a heterogeneous first-order multi-agent system by means of an event-based SMC. This approach is extended to a heterogeneous second-order multi-agent systems in [11], where a novel event-triggered SMC for consensus and formation objectives is implemented.

Knowing the advantages offered by the event-based control techniques, these ones are being applied to multi-robot systems, as in [12], which reports the design of an event-based formation controller applied to terrestrial nonholonomic robots. The works presented in [13] and [14] propose and validate respectively, through simulations and experimental stages, different event-based control strategies for the formation of multiple quadrotors modeled as a second-order multi-agent system. In addition, [15] proves, through simulations the effectiveness of an event-based distributed model predictive control for the formation of multiple UAVs. As it can be noticed, these works address the problem of limited bandwith with different event-based control techniques. However, none of them consider disturbance or model uncertainties, which can lead to instability or deterioration in the performance of the system.

It is then noteworthy that the benefits resulting from the combination of robust control techniques with event-triggered is threefold, i.e. the robustness against disturbances, reduced energy consumption and enhanced inter-vehicles communication. Furthermore, to the best of the authors' knowledge, priorly mentioned works have not presented results regarding collective maneuvering of multiple VTOL rotorcrafts within atmospheric conditions based on similar robust triggered-based control laws.

This paper is an extension of our previous work [16] and it aims at investigating the efficient coordination control of a VTOL rotorcrafts MAS based on a robust event-based control scheme evolving within fluctuating atmospheric conditions. Then, the contributions of this work are summarized next:

- Considering the inner-outer control loop scheme, the presentation of a robust nonlinear quaternion-based controller for attitude stabilization of each VTOL rotorcraft.
- Taking into account the extended translational dynamics entailing unknown disturbances, the synthesis of a robust event-based control scheme for the leader-following consensus of the MAS. The latter is composed of a SMC, featuring an adaptive component and a trigger-mechanism. The novelty of the proposed control law is that it exhibits

[1] J. U. Alvarez-Muñoz and J. Chevalier are with the Robotics Department at EXTIA, Sevres, 92310, France.

[2] J. Escareno, and O. Labanni-Igbida are with the Robotics and Mechatronics Department, XLIM Laboratory UMR CNRS 7252, University of Limoges, France.

[3] S. Daix is with the Computational Fluid Dynamics Department, EXTIA, Sevres, 92310, France

[*] Corresponding author: jalvarezmunoz@extia.fr

robustness against wind-born disturbances, reduced control solicitation and stable inter-vehicles communication. This represents the main contribution of this work.
- The stability of the proposed event-triggered control law is demonstrated via the Lyapunov theory. Furthermore, the used event triggering rule renders the system Zeno free, i.e. sampling is admissible.
- Regarding performance assessment purposes, a detailed 3D simulation scenario including five VTOL rotorcrafts subject to 3D wind-born disturbances intended to reach spatial consensus and formation is carried out.

The sequel of the paper is organised as follows. In Section II, the notation and some mathematical preliminaries used in the manuscript are presented. Section III is devoted to the mathematical modeling of the VTOL-UAV system. Then, section IV explains the attitude control law for each robot, the robust control strategy for position consensus and the formulation of the event-triggered mechanism for the set of aerial vehicles. The simulation scenario and numerical results are presented in Section V. Finally, the conclusions and future works are presented in Section VI.

II. Theoretical Prerequisites

The current section presents the notations and the mathematical background of graph theory and quaternions for attitude representation, which are used in this the paper.

A. Notation

In the following, let $\mathbb{R}^n$ and $\|\cdot\|$ be the $n-$dimensional Euclidean space and the Euclidean norm, respectively. I_N stands for the identity matrix of dimension N. Denote by 1_N a column vector with all entries equal to one. $A \otimes B$ denotes the Kronecker product of matrices A and B. Let $O_{M\times N}$ be a zero matrix of dimension $M \times N$.

B. Graph Theory

A MAS can be modeled as a set of dynamic systems (or agents) in which an information exchange occurs. Such information flow is mathematically represented by means of graph theory. In this regard, [17], [18] establish that a directed graph can be represented as $\mathcal{G} = \{\mathcal{V}, \xi, \mathcal{A}\}$, where $\mathcal{V}$ is a nonempty set containing finite number of vertices or nodes such that $\mathcal{V} = 1, 2, ..., N$ and ξ is an edge set represented as $\xi = (i, j) \forall i, j \in \mathcal{V}$ with (i, j) implies that the node j can obtain information from the node i. $\mathcal{A}$ is the *adjacency* matrix $\mathcal{A} = a(i, j) \in \mathbb{R}^{N\times N}$ where the element $a(i, j)$ is positive if $(i, j) \in \xi$ and it is zero otherwise. $\deg_{in}(i) = \sum_{j=1}^{N} a_{ij}$ is called the in-degree of node i, and $\deg_{out}(i) = \sum_{j=1}^{N} a_{ji}$ is called the out-degree of the node i. The set of neighbors of agent i is denoted by $\mathcal{N}_i = \{j : (i, j) \in \mathcal{V}\}$

The *Laplacian matrix* $\mathcal{L}$ of $\mathcal{G}$ is defined as $\mathcal{L} = \mathcal{D} - \mathcal{A}$, where $\mathcal{D}$ is a diagonal matrix $\mathcal{D} = \text{diag}(d_1, d_2, ...d_n)$ with elements $\sum_{j=1}^{n} a(i, j)$, see [19], [20]. A directed graph is said to have a spanning tree if a node in $\mathcal{V}$ contains directed path to every other distinct node in $\mathcal{V}$. Moreover, if a node set $\mathcal{V} \cup 0$ exists in the directed graph G, describing the interaction between a leader agent 0 and N followers, then $\mathcal{B}$ is a diagonal matrix with entries 1, if there exists an edge between the leader and any other agent in the group, and 0 otherwise.

Lemma II.1. *$\mathcal{G} = \{\mathcal{V}, \xi, \mathcal{A}\}$ is said to be balanced if the in-degree of each node is equal to its out-degree, i.e., $deg_{in}(i) = deg_{out}(i),\ i = 1, 2, ..., N$. It is easy to prove that $\mathcal{G}$ is balanced if and only if $1_N^T \mathcal{L} = 0_N^T$.*

Lemma II.2. *The matrix $\mathcal{L} + \mathcal{B}$ has full rank when $\mathcal{G}$ has a spanning tree with leader as the root, which implies non singularity of $\mathcal{L} + \mathcal{B}$*

Remark II.3. *From here, we shall refer to the matrix $\mathcal{L} + \mathcal{B}$ as $\mathcal{H}$, in order to avoid any confusion.*

C. Unit Quaternion and Attitude Kinematics

Consider a body fixed, main coordinate frame with the orthonormal right handed basis $B(x_b, y_b, z_b)$, and an inertial frame North-East-Down (NED) with basis $N(x_n, y_n, z_n)$. Rigid body rotations in the three dimensional space can be represented without singularity by unit quaternions $q \in \mathbb{S}^3$, defined as:

$$\boldsymbol{q} := \begin{pmatrix} \cos\frac{\beta}{2} \\ \boldsymbol{e}_v \sin\frac{\beta}{2} \end{pmatrix} = \begin{pmatrix} q_0 \\ \boldsymbol{q}_v \end{pmatrix} \in \mathbb{S}^3 \tag{1}$$

where $\boldsymbol{q}_v = (q_1 \ \ q_2 \ \ q_3)^T \in \mathbb{R}^3$ and $q_0 \in \mathbb{R}$ are known as the vector and scalar parts of the quaternion respectively.

Let $\boldsymbol{\omega} = (\omega_1 \ \ \omega_2 \ \ \omega_3)^T$ be the angular velocity vector of the body coordinate frame B, relative to the inertial coordinate frame N, the kinematics equation is given by

$$\begin{pmatrix} \dot{q}_0 \\ \dot{\boldsymbol{q}}_v \end{pmatrix} = \frac{1}{2} \begin{pmatrix} -\boldsymbol{q}_v^T \\ I_3 q_0 + [\boldsymbol{q}_v^\times] \end{pmatrix} \boldsymbol{\omega} = \frac{1}{2} \Xi(\boldsymbol{q}) \boldsymbol{\omega} \tag{2}$$

The rotation matrix R is related to the unit quaternion $\boldsymbol{q}$ through the Rodrigues' formula as:

$$R = (q_0^2 - \boldsymbol{q}_v^T \boldsymbol{q}_v) I_3 + 2 q_0 [\boldsymbol{q}_v^\times] + 2 [\boldsymbol{q}_v^\times]^2 \tag{3}$$

where $[^\times]$ maps the vector to a skew-symmetric matrix.

For two given unit quaternions $\boldsymbol{q}_1$ and $\boldsymbol{q}_2$, the quaternion multiplication can be expressed by:

$$\boldsymbol{q}_1 * \boldsymbol{q}_2 = \begin{pmatrix} q_{01} q_{02} - \boldsymbol{q}_{v1}^T \boldsymbol{q}_{v2} \\ q_{01} \boldsymbol{q}_{v2} + q_{02} \boldsymbol{q}_{v1} + [\boldsymbol{q}_{v2}^\times] \boldsymbol{q}_{v1} \end{pmatrix} \tag{4}$$

with $(*)$ being the quaternion product. Then, the quaternion error $\boldsymbol{q}_e$ is given as the quaternion multiplication of the conjugate of the quaternion $\boldsymbol{q}$ and the desired quaternion $\boldsymbol{q}_d$

$$\boldsymbol{q}_e := \boldsymbol{q}_d^{-1} * \boldsymbol{q} = (q_{e_0} \ \ \boldsymbol{q}_{e_v}^T)^T \tag{5}$$

III. Mathematical Modeling

This section aims to present the overall dynamics of the i^{th} aerial vehicle in the group. Considering that the flight of the multi-UAV system evolves within a real windy environment, aerodynamic forces are produced, which are initially detailed. This forces are taken into account to subsequently present the kinematic and dynamic equations of motion.

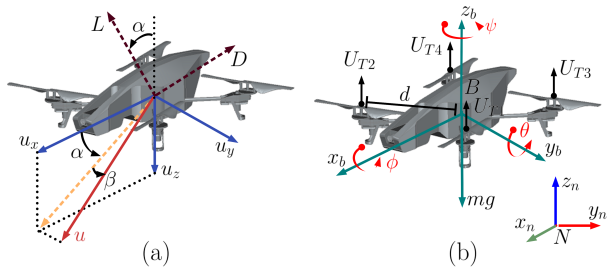

Figure 1: a)Aerodynamic situation. b)Free-body scheme: VTOL rotorcraft

A. Aerodynamics

In order to have a real-world flight envelope, the aerial multi-agent system is exposed to windy conditions. For the aerodynamic analysis, we suppose that every vehicle in the formation is fully submerged within the wind gusts streams.

The wind vector $\boldsymbol{V}_{\omega}^{I} = (\upsilon_{\omega_x}, \upsilon_{\omega_y}, \upsilon_{\omega_z})^T \in \mathbb{R}^3$ used in this work is obtained from the Dryden spectral model [21], [22]. It consists of a static dominant component and a turbulent wind component. Thus, the vertical and horizontal wind components correspond to a summation of sinusoidal functions with random parameters (magnitude, frequency and phase)

$$\upsilon_{\omega_k}(t) = \upsilon_{\omega_k}^{s} + \sum_{j=1}^{n} \sqrt{\triangle_{\omega_j} \Phi_j} \sin(\omega_{n_j} t + \epsilon_j) \text{ with } k : \{x, y, z\} \tag{6}$$

where $\upsilon_{\omega_k}^{s}$ is the static wind, ω_{n_j} is a natural frequency, $\triangle_{\omega_j}$ is frequency samples and Φ_j is a power spectral density.

Considering the vehicles' speeds $\boldsymbol{v}_i$ and the ground wind speed $\boldsymbol{V}_{\omega}^{I}$, both expressed in the inertial frame, the airspeed for each system, expressed in body frame, is given as:

$$\boldsymbol{u} = R^T(\boldsymbol{v} - \boldsymbol{V}_{\omega}^{I}) \tag{7}$$

Now, the airspeed magnitude V, the angle of attack (AoA) α and the sideslip angle β, see Fig. 1, are given as:

$$V = \sqrt{u_x^2 + u_y^2 + u_z^2};\ \alpha = \tan^{-1}\left(\frac{u_z}{u_x}\right);\ \beta = \sin^{-1}\left(\frac{u_y}{V}\right) \tag{8}$$

Finally, the resulting aerodynamic force $\mathrm{W} = (w_x, w_y, w_z)^T$ in its scalar form is:

$$\begin{aligned} w_x &= L\sin\alpha\cos\beta - D\cos\alpha\cos\beta \\ w_y &= L\sin\alpha\sin\beta - D\cos\alpha\sin\beta \\ w_z &= L\cos\alpha + D\sin\alpha \end{aligned} \tag{9}$$

where $L = \frac{1}{2}\rho V^2 S C_L$ and $D = \frac{1}{2}\rho V^2 S C_D$, with S the reference area and C_L and C_D are lift and drag coefficients.

B. Dynamics

In a group of N-VTOL vehicles, each aerial system can be modeled as a rigid body, see Fig. 1. Then, according to [23], the six degrees of freedom model (position and orientation) of the system can be separated into translational and rotational motions, respectively defined by

$$\Sigma_{T_i} : \begin{cases} \dot{\boldsymbol{p}}_i = \boldsymbol{v}_i \\ m_i \dot{\boldsymbol{v}}_i = -m_i \boldsymbol{g} \boldsymbol{e}_{3_i} + U_{T_i} R_i \boldsymbol{e}_{3_i} + \mathrm{W}_i \end{cases} \tag{10}$$

$$\Sigma_{R_i} : \begin{cases} \dot{\boldsymbol{q}} = \frac{1}{2}\Xi(\boldsymbol{q}_i)\boldsymbol{\omega}_i \\ J_i \dot{\boldsymbol{\omega}}_i = -\boldsymbol{\omega}_i^{\times} J_i \boldsymbol{\omega}_i + \boldsymbol{\Gamma}_i + \boldsymbol{d}_i \end{cases} \tag{11}$$

where $i = 1, ..., N$. $\boldsymbol{p}_i$ and $\boldsymbol{v}_i \in \mathbb{R}^3$ are linear positions and velocities vectors, m_i is the mass of each aerial system, $\boldsymbol{g}$ is the mass acceleration, $\boldsymbol{e}_3$ is a unitary vector along the z axis, R is the rotation matrix given in (3), U_{T_i} is the total thrust generated by the four rotors and $\mathrm{W}_i \in \mathbb{R}^3$ corresponds to the disturbance wind vector given in (9). Note that, since the disturbance is produced by static and non-static components of wind, their effects are translated into static $\mathrm{W}_{si} = (w_{sxi}, w_{syi}, w_{szi})^T$ and non-static $\boldsymbol{\Delta}_{W_i} = (\Delta_{W_{xi}}, \Delta_{W_{yi}}, \Delta_{W_{zi}})^T$ forces:

$$\mathrm{W}_i = \mathrm{W}_{si} + \boldsymbol{\Delta}_{W_i} \tag{12}$$

Moreover, it is assumed that the non-static force is bounded in the manner $\|\boldsymbol{\Delta}_{W_i}(t)\| \leq \boldsymbol{\Delta}_{W max_i}$.

$J_i \in \mathbb{R}^{3\times3}$ is the inertia matrix and $\boldsymbol{\Gamma}_i \in \mathbb{R}^3$ is the vector of applied torques, control couples generated by the actuators. Finally, $\boldsymbol{d}_i \in \mathbb{R}^3$ stands for time-varying external disturbances, bounded as $\|\boldsymbol{d}_i\| \leq \boldsymbol{\delta}_i$.

IV. Attitude and Position Control for the VTOL MAS

The current section is divided in two parts. First, we introduce the attitude control law to stabilize the i^{th} agent's attitude. Thus, the position control strategy to achieve consensus to the leader and multi-agent formation is presented.

A. Attitude Control Scheme: Super-Twisting SMC

The aim of the attitude control is to drive the aerial vehicles to attitude stabilization, i.e. to the asymptotic conditions $\boldsymbol{q}_i \to [\pm 1\ 0\ 0\ 0]^T$, $\boldsymbol{\omega_i} \to 0$ as $t \to \infty$. For this, let $\boldsymbol{q}_{d_i} = (q_{di_0}\ \boldsymbol{q}_{di_v})^T$ and $\boldsymbol{\omega}_{di} = (\omega_{1i}\ \ \omega_{2i}\ \ \omega_{3i})^T$ be the desired quaternion and angular velocity. For each aerial vehicle, the quaternion error is given according to (5) and the angular velocity error in terms of quaternions is expressed as

$$\boldsymbol{\omega}_{ei} = \boldsymbol{\omega}_i - R_i \boldsymbol{\omega}_{di} \tag{13}$$

where $\boldsymbol{\omega}_i$ corresponds to the actual orientation of the system and R_i is the rotation matrix given by (3). Then, by calculating the time derivative of the quaternion error and the angular velocity error, the attitude error dynamics can be given by

$$\begin{pmatrix} \dot{q}_{ei_0} \\ \dot{\boldsymbol{q}}_{ei_v} \end{pmatrix} = \frac{1}{2}\begin{pmatrix} -\boldsymbol{q}_{ei_v}^T \\ I_3 q_{ei_0} + [\boldsymbol{q}_{ei_v}^{\times}] \end{pmatrix} \boldsymbol{\omega}_{ei} \tag{14}$$

$$\dot{\boldsymbol{\omega}}_{ei} = \boldsymbol{\omega}_{ei}^{\times} R_i \boldsymbol{\omega}_{di} - R_i \dot{\boldsymbol{\omega}}_{di} - J_i^{-1} \boldsymbol{\omega}_{ei}^{\times} J_i \boldsymbol{\omega}_{ei} + J_i^{-1} \boldsymbol{\Gamma}_i + J_i^{-1} \boldsymbol{d}_i \tag{15}$$

The design of the attitude control law consists of a robust Super Twisting sliding mode control, where the sliding surface and its time derivative are computed as follows

$$\boldsymbol{s}_i = J_i \boldsymbol{\omega}_{ei} + \lambda_i \boldsymbol{q}_{ei_v} + \kappa_i \boldsymbol{\varepsilon}_i \tag{16}$$

$$\dot{\boldsymbol{s}}_i = J_i \dot{\boldsymbol{\omega}}_{ei} + \lambda_i \dot{\boldsymbol{q}}_{ei_v} + \kappa_i \boldsymbol{q}_{ei_v} \tag{17}$$

where $\boldsymbol{s}_i \in \mathbb{R}^3$ and $\boldsymbol{\varepsilon_i} \in \mathbb{R}^3$ corresponds to the integral of the error in terms of quaternions. Besides, $\lambda_i > 0,\ \kappa_i \geq 0 \in \mathbb{R}^{3\times3}$ are diagonal matrices standing as control tuning parameters. Then, by substituting equation (15) into (17), allows to stabilize the attitude dynamics via a Super Twisting SMC scheme, i.e.

$$\begin{aligned}\boldsymbol{\Gamma}_i = &- J_i(\boldsymbol{\omega}_{ei}^{\times} R_i \boldsymbol{\omega}_{di} - R_i\dot{\boldsymbol{\omega}}_{di}) + \boldsymbol{\omega}_{ei}^{\times} J_i \boldsymbol{\omega}_{ei} \\ &- \lambda_i \dot{\boldsymbol{q}}_{ei_v} - \kappa_i \boldsymbol{q}_{ei_v} - k_{1i}|\boldsymbol{s}_i|^{\frac{1}{2}}\text{sign}(\boldsymbol{s}_i) \\ &- k_{2i}\int_0^t \text{sign}(\boldsymbol{s}_i)d\tau - a_i\text{sign}(\boldsymbol{s}_i)\end{aligned} \tag{18}$$

where $k_i > 0 \in \mathbb{R}^{3\times3}$ are diagonal matrices being the super twisting gains. $a\text{sign}(\boldsymbol{s}_i)$ is a reaching law with $a > 0 \in \mathbb{R}^{3\times3}$ a diagonal matrix, used similarly to [16]. With this, the closed loop error dynamics $\dot{\boldsymbol{s}}_i$ is given by

$$\dot{\boldsymbol{s}}_i = -k_{1i}|\boldsymbol{s}_i|^{\frac{1}{2}}\text{sign}(\boldsymbol{s}_i) - k_{2i}\int_0^t \text{sign}(\boldsymbol{s}_i)d\tau - a_i\text{sign}(\boldsymbol{s}_i) + \boldsymbol{d}_i \tag{19}$$

Now, let us introduce the state vector $\boldsymbol{\chi} = (\chi_{1i}\ \chi_{2i})^T$. Then, computing its time derivative and writing it the scalar form we can obtain:

$$\begin{aligned}\dot{\boldsymbol{\chi}}_{1i} &= -k_{1i}|\boldsymbol{\chi}_{1i}|^{\frac{1}{2}}\text{sign}(\boldsymbol{\chi}_{1i}) + \boldsymbol{\chi}_{2i} \\ \dot{\boldsymbol{\chi}}_{2i} &= -k_{2i}\text{sign}(\boldsymbol{\chi}_{1i}) + \boldsymbol{d}_i(t,\boldsymbol{\chi})\end{aligned} \tag{20}$$

Proof. Consider the next Lyapunov function given in [24], [25] as:

$$V(\boldsymbol{\chi}) = \boldsymbol{\zeta}^T P \boldsymbol{\zeta} \tag{21}$$

where $\boldsymbol{\zeta} = (|\boldsymbol{\chi}|_1^{\frac{1}{2}}\text{sign}(\boldsymbol{\chi}_1)\ \boldsymbol{\chi}_2)^T$. $P = P^T$ is a positive definite matrix, and its construction is based on the next matrix inequality (MI):

$$\begin{pmatrix} A^TP + PA + \epsilon P + \delta^2 C^T C & P\boldsymbol{B} \\ \boldsymbol{B}^T P & -1 \end{pmatrix} \leq 0 \tag{22}$$

where

$$A = \begin{pmatrix} -\frac{1}{2}k_1 & \frac{1}{2} \\ -k_2 & 0 \end{pmatrix};\quad \boldsymbol{B} = \begin{pmatrix} 0 \\ 1 \end{pmatrix};\quad \boldsymbol{C} = \begin{pmatrix} 1 & 0 \end{pmatrix}; \tag{23}$$

with $\epsilon > 0$. Then, the time derivative of the Lyapunov function is:

$$\dot{V}(\boldsymbol{\chi}) = \frac{1}{|\boldsymbol{\zeta}|}\{\boldsymbol{\zeta}^T(A^TP + PA)\boldsymbol{\zeta} + \tilde{\boldsymbol{d}}^T\boldsymbol{B}^TP\boldsymbol{\zeta} + \boldsymbol{\zeta}^TP\boldsymbol{B}\tilde{\boldsymbol{d}}\} \tag{24}$$

Finally, after some manipulations, it can be concluded that $\dot{V}(\boldsymbol{\chi})$ satisfies:

$$\dot{V}(\boldsymbol{\chi}) \leq -\frac{\epsilon}{|\zeta_1|}\boldsymbol{\zeta}^TP\boldsymbol{\zeta} \leq -\epsilon\lambda_{min}^{\frac{1}{2}}PV^{\frac{1}{2}}(\boldsymbol{\chi}) \tag{25}$$

Then, it can be shown that the state converges to zero in finite time, as it is detailed in [24], [25].

□

B. Position Control Scheme: Event-based Adaptive SMC

The MAS control strategy proposed herein is intended to fulfill the consensus objective while rejecting wind-born disturbances. Generally speaking, considering a virtual leader, the MAS must achieve a leader-following consensus, i.e.

$$\lim_{t\to\infty} ||\boldsymbol{p}_i - \boldsymbol{1}_N \otimes \boldsymbol{p}_0|| \to 0 \tag{26}$$

where $\boldsymbol{p}_i \in \mathbb{R}^{mN}$ and $\boldsymbol{p}_0 \in \mathbb{R}^m$ ($m = 3$ for our case) are the position vectors of the ith follower and the virtual leader, respectively. Let the ith rotorcraft translational dynamics (10) be rewritten as:

$$\dot{\boldsymbol{p}}_i = \begin{pmatrix} \dot{p}_{x_i} \\ \dot{p}_{y_i} \\ \dot{p}_{z_i} \end{pmatrix} = \begin{pmatrix} v_{x_i} \\ v_{y_i} \\ v_{z_i} \end{pmatrix}, \tag{27}$$

$$\dot{\boldsymbol{v}}_i = \begin{pmatrix} \dot{v}_{x_i} \\ \dot{v}_{y_i} \\ \dot{v}_{z_i} \end{pmatrix} = \begin{pmatrix} \frac{U_{T_i}}{m_i}(\text{C}_{\psi_i}\text{S}_{\theta_i}\text{C}_{\phi_i} + \text{S}_{\psi_i}\text{S}_{\theta_i}) + w_{xi} \\ \frac{U_{T_i}}{m_i}(\text{S}_{\psi_i}\text{S}_{\theta_i}\text{C}_{\phi_i} - \text{C}_{\psi_i}\text{S}_{\phi_i}) + w_{yi} \\ \frac{U_{T_i}}{m_i}(\text{C}_{\phi_i}\,\text{C}_{\theta_i}) - g + w_{zi} \end{pmatrix} \tag{28}$$

where $\text{S}_\star$ and $\text{C}_\star$ stand for $\sin(\star)$ and $\cos(\star)$, respectively.

For control purposes, let the virtual control inputs be defined as follows

$$\begin{cases} V_{x_i} = \frac{U_{T_i}}{m_i}(\text{C}_{\psi_i}\text{S}_{\theta_i}\text{C}_{\phi_i} + \text{S}_{\psi_i}\text{S}_{\theta_i}) \\ V_{y_i} = \frac{U_{T_i}}{m_i}(\text{S}_{\psi_i}\text{S}_{\theta_i}\text{C}_{\phi_i} - \text{C}_{\psi_i}\text{S}_{\phi_i}) \\ V_{z_i} = \frac{U_{T_i}}{m_i}(\text{C}_{\phi_i}\,\text{C}_{\theta_i}) - g \end{cases} \tag{29}$$

Hence, the desired Euler angles (θ_{di}, ϕ_{di}) and the total thrust U_{T_i} can be obtained as

$$\begin{cases} U_{Ti} = m\sqrt{V_{x_i}^2 + V_{y_i}^2 + (V_{z_i} + g)^2} \\ \phi_{di} = \arctan(\text{C}_{\theta_{di}}(\frac{V_{x_i}\text{S}_{\psi_{di}} - V_{y_i}\text{C}_{\psi_{di}}}{V_{z_i}+g})) \\ \theta_{di} = \arctan(\frac{V_{x_i}\text{C}_{\psi_{di}} + V_{y_i}\text{S}_{\psi_{di}}}{V_{z_i}+g}) \end{cases} \tag{30}$$

where ψ_{di} is the desired yaw angle.

Now, let us introduce the lumped tracking errors for the ith aerial robot, which in terms of graph theory are given as

$$\begin{aligned}\boldsymbol{e}_{p_i}(t) &= (\mathcal{L} + \mathcal{B}) \otimes I_3\bar{\boldsymbol{p}}(t) = \mathcal{H} \otimes I_3\bar{\boldsymbol{p}}_i(t) \in \mathbb{R}^{3N} \\ \boldsymbol{e}_{v_i}(t) &= (\mathcal{L} + \mathcal{B}) \otimes I_3\bar{\boldsymbol{v}}_i(t) = \mathcal{H} \otimes I_3\bar{\boldsymbol{v}}(t) \in \mathbb{R}^{3N}\end{aligned} \tag{31}$$

where matrix $\mathcal{B} = \text{diag}(b_1, \ldots, b_N)$ indicates the MAS members receiving the navigation protocol (leader). Additionally:

- $\boldsymbol{e}_{p_i}(t) = (\boldsymbol{e}_{p1}^T(t), ..., \boldsymbol{e}_{pN}^T(t))^T$,
- $\boldsymbol{e}_{v_i}(t) = (\boldsymbol{e}_{v1}^T(t), ..., \boldsymbol{e}_{vN}^T(t))^T$,
- $\bar{\boldsymbol{p}}_i(t) = \boldsymbol{p}_i(t) - \boldsymbol{1}_N \otimes \boldsymbol{p}_0(t)$,
- $\bar{\boldsymbol{v}}_i(t) = \boldsymbol{v}_i(t) - \boldsymbol{1}_N \otimes \dot{\boldsymbol{p}}_0(t)$,
- $\boldsymbol{p}_i(t) = (\boldsymbol{p}_1^T(t), ..., \boldsymbol{p}_N^T(t))^T$,
- $\boldsymbol{v}_i(t) = (\boldsymbol{v}_1^T(t), ..., \boldsymbol{v}_N^T(t))^T$,
- $\boldsymbol{u}_i(t) = (\boldsymbol{u}_1^T(t), ..., \boldsymbol{u}_N^T(t))^T$,
- $\text{W}_i(t) = (\text{W}_1^T(t), ..., \text{W}_N^T(t))^T$

Then, the time derivative of (31) can be expressed by

$$\begin{aligned}\dot{\boldsymbol{e}}_{p_i} &= \boldsymbol{e}_{v_i} \\ \dot{\boldsymbol{e}}_{v_i} &= \mathcal{H} \otimes I_3 \cdot (\boldsymbol{u}_i(t) - 1_N \otimes \ddot{\boldsymbol{p}}_0(t) + \text{W}_i(t))\end{aligned} \tag{32}$$

To mitigate the wind-born disturbances degrading the MAS leader-based consensus, a wind-tolerant control law is synthesized.

- The static wind component engenders a slow time-varying force $\mathrm{W}_{si}(t)$, considered unknown but assumed bounded. Then, the latter is compensated with its estimated value $\hat{\mathrm{W}}_{si}(t) = (\hat{w}_{xsi}(t), \hat{w}_{ysi}(t), \hat{w}_{zsi}(t))^T$, defining the estimation error and its derivative as

$$\begin{aligned} \tilde{\mathrm{W}}_{si}(t) &\triangleq \hat{\mathrm{W}}_{si}(t) - \mathrm{W}_{si}(t) \\ \dot{\tilde{\mathrm{W}}}_{si}(t) &= \dot{\hat{\mathrm{W}}}_{si}(t) \end{aligned} \tag{33}$$

  assuming small magnitude fluctuations of $\mathrm{W}_{si}(t)$, it is thus assumed that $\dot{\mathrm{W}}_{si}(t) \approx 0$.
- The SMC technique is known for its inherent robustness, it provides the framework to deal with time-varying disturbances. Regarding our scenario, it corresponds to disturbances arising from the non-static wind $\boldsymbol{\Delta}_{W_i}(t)$

From the latter, a sliding surface is then proposed to meet the MAS consensus performance criteria,

$$\boldsymbol{S}_i(t) = \boldsymbol{e}_{v_i}(t) + \lambda \boldsymbol{e}_{p_i}(t) \tag{34}$$

where $\lambda = \mathrm{diag}(\mathrm{diag}(\lambda_{x_1}, \lambda_{y_1}, \lambda_{z_1}), \ldots, \mathrm{diag}(\lambda_{x_N}, \lambda_{y_N}, \lambda_{z_N})$, $\lambda \in \mathbb{R}^{3N\times 3N}$, denotes the control gain matrix. Similarly to [26], the control input proposed for the system is expressed by:

$$\begin{aligned} \boldsymbol{u}_i(t) = \quad & \mathcal{H}^{-1} \otimes I_3 \cdot \big(- K_s \mathbf{tanh}^{\star}(\boldsymbol{S}_i(t)) - \lambda \boldsymbol{e}_{v_i}(t) \\ & + \mathcal{B} \otimes I_3 \cdot \mathbf{1}_N \otimes \ddot{\boldsymbol{p}}_0(t) - \mathcal{H} \otimes I_3 \cdot \hat{\mathrm{W}}_{s_i}(t) \big) \end{aligned} \tag{35}$$

with $K_s = \mathrm{diag}(K_{s_1}, \ldots, K_{s_N}) \otimes I_3$, $K_s \in \mathbb{R}^{3N\times 3N}$, is a positive-definite diagonal matrix. Let the adaptation law be expressed as:

$$\dot{\hat{\mathrm{W}}}_{s_i}(t) = K_a \cdot \mathcal{H} \otimes I_3 \cdot \boldsymbol{S}_i(t) \tag{36}$$

where $K_a = \mathrm{diag}(K_{a_1}, \ldots, K_{a_N}) \otimes I_3$, $K_a \in \mathbb{R}^{3N\times 3N}$.

Remark IV.1. *To alleviate inherent SMC-due chattering, the hyperbolic function tanh($\boldsymbol{S}(t)$) is used. Moreover, the stability analysis is done accordingly.*

Event-based scheme suits to collective and cooperative tasks that relies on effective MAS communication while featuring limited resources (bandwidth and processing). Hence, the sampled control input is updated only when an event occurs. In consequence, data traffic network and power consumption are diminished. Then, the control law $\boldsymbol{u}(t)$ given in (35) is modified in such a way that $\forall\ t\ \in\ [t^k, t^{k+1})$

$$\begin{aligned} \boldsymbol{u}_i(t) = \quad & \mathcal{H}^{-1} \otimes I_3 \cdot \big(- K_s \mathbf{tanh}^{\star}(\boldsymbol{S}_i(t^k)) - \lambda \boldsymbol{e}_{v_i}(t^k) \\ & + \mathcal{B} \otimes I_3 \cdot \mathbf{1}_N \otimes \ddot{\boldsymbol{p}}_0(t^k) - \mathcal{H} \otimes I_3 \cdot \hat{\mathrm{W}}_{s_i}(t^k) \big) \end{aligned} \tag{37}$$

where $\mathbf{tanh}^{\star}(\boldsymbol{S}_i(t^k))$ verifies the following

$$\mathbf{tanh}^{\star}(\cdot) = \begin{cases} \mathbf{tanh}(\boldsymbol{S}_i(t^k)) \text{ if } \|\mathbf{tanh}(\boldsymbol{S}_i(t^k))\| < |\frac{\kappa}{\lambda_m\{K_s\}}| \\ \frac{\kappa}{\lambda_m\{K_s\}} \text{ if } \|\mathbf{tanh}(\boldsymbol{S}_i(t^k))\| \geq |\frac{\kappa}{\lambda_m\{K_s\}}| \end{cases} \tag{38}$$

where $\lambda_m\{K_s\}$ represents a matrix's minimal eigenvalue and $\lambda_m\{K_s\} > \kappa$. Sampling errors arise due to the discretization process of the controller, these are expressed as

$$\begin{aligned} \bar{\boldsymbol{\epsilon}}_{p_i}(t) &= \boldsymbol{p}_i(t) - \boldsymbol{p}_i(t^k) \\ \bar{\boldsymbol{\epsilon}}_{v_i}(t) &= \boldsymbol{v}_i(t) - \boldsymbol{v}_i(t^k) \\ \bar{\boldsymbol{\epsilon}}_{u_0}(t) &= \ddot{\boldsymbol{p}}_0(t) - \ddot{\boldsymbol{p}}_0(t^k) \end{aligned} \tag{39}$$

such that at t^k, $\bar{\boldsymbol{\epsilon}}(t) = 0$. Note that t_i^k corresponds to the triggering instant of the ith agent. Hence, $\bar{\boldsymbol{\epsilon}}_i(t)$ and $\bar{\boldsymbol{\epsilon}}_0(t)$ denotes the discretization error between the agents and leader, respectively. Likewise, it is possible to rewrite the lumped errors as

$$\begin{aligned} \bar{\boldsymbol{e}}_{p_i}(t) &= \boldsymbol{e}_{p_i}(t) - \boldsymbol{e}_{p_i}(t^k) \\ \bar{\boldsymbol{e}}_{v_i}(t) &= \boldsymbol{e}_{v_i}(t) - \boldsymbol{e}_{v_i}(t^k) \end{aligned} \tag{40}$$

Theorem IV.2. *Considering the system described by (27-28), with error variables (31) and (39-40), sliding manifold $S(t)$ in the notions of sliding mode and the control law (37)*

- *The convergence to the sliding manifold is confirmed for some reachability constant $\kappa > 0$*
- *The event-based sliding mode control law (37) provides stability in the sense of Lyapunov if the gain K_s accomplishes*

$$\begin{aligned} \kappa \geq sup\Big\{ & (\mathcal{H} \otimes I_3) \cdot \big(\boldsymbol{\Delta}_{W max}(t) - \|1_N \otimes (\boldsymbol{\epsilon}_{u_0}(t))\| \big) \\ & + |\lambda| \|\bar{\boldsymbol{e}}_{v_i}(t)\| \Big\} \end{aligned} \tag{41}$$

Proof. Let a candidate Lyapunov function be given by:

$$V = \frac{1}{2} \boldsymbol{S}_i^T(t) \boldsymbol{S}_i(t) + \frac{1}{2} \tilde{\mathrm{W}}_{s_i}^T(t) K_a^{-1} \tilde{\mathrm{W}}_{s_i}(t) \tag{42}$$

where the adaptation gain K_a is defined in (36). From (42), the time derivative of $\boldsymbol{V}$ is obtained as follows:

$$\begin{aligned} \dot{V} = & \boldsymbol{S}_i^T(t) \big\{ H \otimes I_3 \cdot \big(\boldsymbol{u}_i(t) - \mathbf{1}_N \otimes \ddot{\boldsymbol{p}}_0(t) + \mathrm{W}_i(t) \big) \\ & + \lambda \boldsymbol{e}_{v_i}(t) \big\} + \tilde{\mathrm{W}}_{s_i}^T(t) K_a^{-1} \dot{\tilde{\mathrm{W}}}_{s_i}(t) \end{aligned} \tag{43}$$

Introducing the control law (37) yields

$$\begin{aligned} \dot{V} = & \boldsymbol{S}_i^T(t) \Big\{ \mathcal{H} \otimes I_3 \cdot \Big[\mathcal{H}^{-1} \otimes I_3 \cdot \big(- K_s \mathbf{tanh}^{\star}(\boldsymbol{S}_i(t^k)) \\ & - \lambda \boldsymbol{e}_{v_i}(t^k) + \mathcal{B} \otimes I_3 \cdot \mathbf{1}_N \otimes \ddot{\boldsymbol{p}}_0(t^k) - \mathcal{H} \otimes I_3 \cdot \hat{\mathrm{W}}_{s_i}(t^k) \big) \\ & - 1_N \otimes \ddot{\boldsymbol{p}}_0(t) + \mathrm{W}_i(t) \Big] + \lambda \boldsymbol{e}_{v_i}(t) \Big\} + \tilde{\mathrm{W}}_{s_i}^T(t) K_a^{-1} \dot{\hat{\mathrm{W}}}_{s_i}(t) \\ = & \boldsymbol{S}_i^T(t) \Big\{ \lambda \boldsymbol{e}_{v_i}(t) - \lambda \boldsymbol{e}_{v_i}(t^k) - K_s \mathbf{tanh}^{\star}(\boldsymbol{S}_i(t^k)) \\ & + \mathcal{H} \otimes I_3 \cdot \Big(\mathrm{W}_{s_i}(t) + \boldsymbol{\Delta}_{W_i}(t) - \mathbf{1}_N \otimes (\ddot{\boldsymbol{p}}_0(t) - \ddot{\boldsymbol{p}}_0(t^k)) \\ & - \hat{\mathrm{W}}_{s_i}(t^k) \Big) \Big\} + \tilde{\mathrm{W}}_{s_i}^T(t) K_a^{-1} \dot{\hat{\mathrm{W}}}_{s_i}(t) \\ = & \boldsymbol{S}_i^T(t) \Big\{ \lambda (\boldsymbol{e}_{v_i}(t) - \boldsymbol{e}_{v_i}(t^k)) - K_s \mathbf{tanh}^{\star}(\boldsymbol{S}_i(t^k)) \\ & + \mathcal{H} \otimes I_3 \cdot \Big(\mathrm{W}_{s_i}(t) + \boldsymbol{\Delta}_{W_i}(t) - \hat{\mathrm{W}}_{s_i}(t^k) - \mathbf{1}_N \otimes \boldsymbol{\epsilon}_{u_0}(t) \Big) \Big\} \\ & + \tilde{\mathrm{W}}_{s_i}^T(t) \cdot \mathcal{H} \otimes I_3 \cdot \boldsymbol{S}_i^T(t^k) \end{aligned}$$

where we have used (12) and (36). Now, using (**??**), (39).c and the prior mentioned $\dot{\mathrm{W}}_{s_i}(t) \approx 0$, implying $\dot{\hat{\mathrm{W}}}_{s_i}(t^k) \approx \dot{\hat{\mathrm{W}}}_{s_i}(t)$, also, considering (41) lead us to

$$\begin{aligned} \dot{V} \leq & \|\boldsymbol{S}_i^T(t)\| \Big(\kappa - \lambda_m\{K_s\} \|\mathbf{tanh}^{\star}(\boldsymbol{S}_i(t^k))\| \Big) \\ & - \boldsymbol{S}_i^T(t) \big(\|\mathcal{H} \otimes I_3\| \cdot (\tilde{\mathrm{W}}_{s_i}(t) - \tilde{\mathrm{W}}_{s_i}(t)) \big) \end{aligned} \tag{44}$$

Thus, the state trajectories are in the neighboring of the sliding manifold, it yields

$$\dot{V} \leq \|\boldsymbol{S}_i^T(t)\| \Big(\kappa - \lambda_m\{K_s\} \|\mathbf{tanh}^{\star}(\boldsymbol{S}_i(t))\| \Big)$$

Now, it is possible to verify that the Lyapunov function is semi-definite negative (see 38). Actually, it implies that there is an attractive manifold in the origin's neighborhood

$$\Omega = \left\{ \boldsymbol{S(t)} \in \mathbb{R}^{3N} : \dot{V} = 0 \text{ for } \|\mathbf{tanh}(\boldsymbol{S}(t)_i)\| = |\tfrac{\kappa}{\lambda_m\{K_s\}}| \right\} \tag{45}$$

such as the state vector remains bounded. Thus, the sliding manifold contained in Ω is an attractor and the vector state trajectories remains arbitrarily close to it $\forall \ \in \ [t^k, t^{k+1})$.

□

Remark IV.3. *Note that during the interval $[t^k, t^{k+1})$ the states trajectories move away the sliding manifold $\boldsymbol{S}(t)$ till the next triggering occurs. However, it remains bounded in the vicinity of the manifold, where the band size is independent of sampling interval and disturbance bound. Thus, the system is said to be in practical sliding mode.*

The time t^k at which an event is triggered is described by a trigger mechanism. In other words, as long as a criterion (established by the trigger mechanism) is respected, the next event is not triggered and the control signal keeps its prior value constant. Let the trigger mechanism be expressed as

$$\xi = \|\nu_{1_i} \boldsymbol{e}_{pi} + \nu_{2_i} \boldsymbol{e}_{vi}\| - \boldsymbol{\delta}_i \tag{46}$$

with $\nu_1 > 0$, $\nu_2 > 0$ diagonal matrices and $\boldsymbol{\delta}_i \in \mathbb{R}_+$. Both, errors in position and velocity are taken into consideration by the triggering rule to ensure a stable closed-loop performance. Additionally, $(\boldsymbol{\delta}_i)$ corresponds to a state independent threshold, which ensures a finite positive lower bound between any two consecutive triggering instants, thereby excluding Zeno behavior, i.e. no two consecutive events occur at the same time.

Theorem IV.4. *Consider the group of mini aerial vehicles described by (27-28), with the control law (37) and the discretization error given in (39). Let the triggering sequences $(t_i^k)_{k=0}^{\infty}$ for the aerial vehicles satisfy the triggering rule given by (46). Then, the inter-event execution $T_i^k = t_i^{k+1} - t_i^k$ is lower bounded by a positive value ϑ, and Zeno behavior is avoided.*

Assumption IV.5. *A function $f(\cdot)$ satisfies the Lipschitz condition over a domain $\mathbb{R}^d$, if for every $R > 0$ there exists a constant $L > 0$ such that*

$$\|f(x_1) - f(x_2)\| \leq L\|x_1 - x_2\| \tag{47}$$

$\forall x_1, x_2 \in \mathbb{R}^d$ such that $\|x_1\|, \|x_2\| \leq R$. L is denoted as the Lipschitz constant for $f(\cdot)$

Proof. Recall the control protocol given in (37) for each vehicle, which can be rewritten as

$$\begin{aligned} \boldsymbol{u}_i(t) =& \mathcal{H}^{-1} \otimes I_3 \cdot \big(\mathcal{B} \otimes I_3 \cdot \mathbf{1}_N \otimes \ddot{\boldsymbol{p}}_0(t^k) - \tilde{\lambda} f(\boldsymbol{X}_i(t^k)) \\ &+ \lambda \boldsymbol{v}_0(t^k) - K_s \mathbf{tanh}^{\star}(\boldsymbol{S}_i(t^k)) \big) \end{aligned} \tag{48}$$

with

$$f(\boldsymbol{X}_i(t^k)) = \begin{pmatrix} \boldsymbol{v}_i(t^k) \\ \mathcal{H} \otimes I_3 \cdot \hat{\mathrm{W}}_{s_i}(t^k) \end{pmatrix} \in \mathbb{R}^{6N},$$

$$\tilde{\lambda} = \begin{pmatrix} (\lambda_1 \ I_3) & O_{3\times 6} & \dots & O_{3\times 6} \\ O_{3\times 6} & (\lambda_2 \ I_3) & \ddots & \vdots \\ \vdots & \ddots & \ddots & O_{3\times 6} \\ O_{3\times 6} & \dots & O_{3\times 6} & (\lambda_N \ I_3) \end{pmatrix} \in \mathbb{R}^{3N\times 6N}$$

Now, let us define a state vector $\boldsymbol{X}_i = (\boldsymbol{p}_i, \boldsymbol{v}_i)^T \in \mathbb{R}^{6N}$. Then, the collective behavior of the group of UAV's from system (27-28) can be expressed as

$$\dot{\boldsymbol{X}}_i(t) = f(\boldsymbol{X}_i(t)) + I_N \otimes \bar{B} \cdot (\boldsymbol{u}_i(t) + \boldsymbol{\Delta}_{W_i}(t)) \tag{49}$$

where $f(\boldsymbol{X}_i(t)) = (\boldsymbol{v}_i(t), \mathrm{W}_{s_i}(t))^T \in \mathbb{R}^{6N}$, $\bar{B} = (O_{3\times 3}, I_3)^T \in \mathbb{R}^{3\times 6}$. Even more, considering (40), let us define an error state vector as

$$\hat{\boldsymbol{\epsilon}}_i(t) = (\bar{\boldsymbol{\epsilon}}_{p_i}(t), \bar{\boldsymbol{\epsilon}}_{v_i}(t))^T \in \mathbb{R}^{6N} \tag{50}$$

Taking now the inter-event execution time as $T_i^k = t_i^{k+1} - t_i^k$, as the time it takes for $||\hat{\boldsymbol{\epsilon}}_i(t)||$ to rise from 0 to $||\hat{\boldsymbol{\epsilon}}_i(t)||_{\infty}$ for the $(k+1)^{th}$ execution of the control signal (37). Then, between k^{th} and $(k+1)^{th}$ the sampling instant in the execution of control, the discretization error is non zero. Now $\forall \ t \ \in [t^k, t^{k+1})$

$$\begin{aligned} &\frac{d}{dt}||\hat{\boldsymbol{\epsilon}}_i(t)|| \leq \left\| \frac{d}{dt} \hat{\boldsymbol{\epsilon}}_i(t) \right\| \leq \left\| \frac{d}{dt} \boldsymbol{X}_i(t) \right\| \\ &\left\| \frac{d}{dt} \hat{\boldsymbol{\epsilon}}_i(t) \right\| \leq \left\| f(\boldsymbol{X}_i(t)) + I_N \otimes \bar{B} \cdot (\boldsymbol{u}_i(t) + \boldsymbol{\Delta}_{W_i}(t)) \right\| \end{aligned} \tag{51}$$

Substituting the control law (48) in the inequality, we obtain

$$\begin{aligned} \leq& \|f(\boldsymbol{X}_i(t)) + I_N \otimes \bar{B} \cdot \big(\mathcal{H}^{-1} \otimes I_3 \cdot (\mathcal{B} \otimes I_3 \cdot \mathbf{1}_N \otimes \ddot{\boldsymbol{p}}_0(t^k) \\ &- \tilde{\lambda} f(\boldsymbol{X}_i(t^k)) + \lambda \boldsymbol{v}_0(t^k) - K_s \mathbf{tanh}^{\star}(\boldsymbol{S}_i(t^k))) + \boldsymbol{\Delta}_{W_i}(t) \big) \| \\ \leq& \|f(\boldsymbol{X}_i(t))\| + \|\Pi \mathcal{B} \otimes I_3 \cdot \mathbf{1}_N \otimes \ddot{\boldsymbol{p}}_0(t^k)\| \\ &+ \|\Pi \tilde{\lambda} f(\boldsymbol{X}_i(t^k))\| + \|\Pi \lambda \boldsymbol{v}_0(t^k)\| + \|\Pi K_s \mathbf{tanh}^{\star}(\boldsymbol{S}_i(t^k))\| \\ &+ \|I_N \otimes \bar{B} \cdot \boldsymbol{\Delta}_{W_i}(t)\| \end{aligned} \tag{52}$$

where $\Pi = (I_N \mathcal{H}^{-1}) \otimes (\bar{B} I_3)$. Further simplifications lead us to

$$\begin{aligned} &\leq L\|\boldsymbol{X}_i(t)\| + \|\Pi\tilde{\lambda}\| L \|\boldsymbol{X}_i(t^k)\| + \Phi \\ &\leq L\|\boldsymbol{X}_i(t^k) + \hat{\boldsymbol{\epsilon}}_i(t)\| + \|\Pi\tilde{\lambda}\| L \|\boldsymbol{X}_i(t^k)\| + \Phi \\ &\leq L\|\hat{\boldsymbol{\epsilon}}_i(t)\| + L(I_N + \|\Pi\tilde{\lambda}\|)\|\boldsymbol{X}_i(t^k)\| + \Phi \\ &\leq L\|\hat{\boldsymbol{\epsilon}}_i(t)\| + \Phi + \Theta \end{aligned} \tag{53}$$

with

$$\begin{aligned} \Phi =& \|\Pi \mathcal{B} \otimes I_3 \cdot \mathbf{1}_N \otimes \ddot{\boldsymbol{p}}_0(t^k)\| + \|\Pi \lambda \boldsymbol{v}_0(t^k)\| \\ &+ \|\Pi K_s \mathbf{tanh}^{\star}(\boldsymbol{S}_i(t^k))\| + \|I_N \otimes \bar{B} \cdot \boldsymbol{\Delta}_W(t)\| \\ \Theta =& L(I_N + \|\Pi\tilde{\lambda}\|)\|\boldsymbol{X}(t^k)\| \end{aligned}$$

One way to understand the solution of the differential inequality (53) for $[t^k, t^{k+1})$, is by invoking the Comparison Lemma [27] and setting the initial condition $\|\hat{\boldsymbol{\epsilon}}_i(t)\| = 0$. It can be easily verified that Θ is non zero for $\|\boldsymbol{X}_i(t^k)\| \neq 0$ as the system is asymptotically stable. Furthermore, the quantities in Φ are also positives. Hence, it is possible to verify that T_i^k is always bounded below by a positive value ϑ so that

$$\|\hat{\boldsymbol{\epsilon}}_i(t)\| \leq \vartheta \tag{54}$$

which allows to end the proof. □

C. Formation Control

The control law (37) allows the convergence to zero between followers and leader. However, if the objective is to obtain geometrical patterns completed by the group of vehicles, then, the consensus can be extended to formation control. Since the followers move towards the virtual leader, a desired distance must be considered to achieve and maintain the formation. Then, let us define Λ as a feasible formation such that

$$\Lambda = \{\boldsymbol{\mu}_{ij} \in \mathbb{R} |\ \boldsymbol{\mu}_{ij} > 0; \quad i, j = 1, ..., N\} \tag{55}$$

where $\boldsymbol{\mu}_{ij} = \boldsymbol{\mu}_{ji} = \|\boldsymbol{\chi}_i - \boldsymbol{\chi}_j\|$ describe the inter-agent and leader-follower distances. To attain the desired formation, let the desired points in the space be defined by a set as

$$\mathcal{Q} = \{\boldsymbol{\chi}_1, ..., \boldsymbol{\chi}_n\},\ \boldsymbol{\chi}_i \in \mathbb{R}^3 \tag{56}$$

With this, the tracking errors (31) can be extended in the following manner:

$$\begin{aligned} \boldsymbol{e}_{p_i}(t) &= \mathcal{H} \otimes I_3 \cdot (\boldsymbol{p}_i(t) - \mathbf{1}_N \otimes \boldsymbol{p}_0(t) - \boldsymbol{\mu}_i) \in \mathbb{R}^{3N} \\ \boldsymbol{e}_{v_i}(t) &= \mathcal{H} \otimes I_3 \cdot \bar{\boldsymbol{v}}(t) \in \mathbb{R}^{3N} \end{aligned} \tag{57}$$

where $\boldsymbol{\mu}_i(t) = (\boldsymbol{\mu}_1^T(t), ..., \boldsymbol{\mu}_N^T(t))^T$

Remark IV.6. *Once the tracking errors given by (57) are considered, the control design methodology follows the same steps as the ones presented in subsection IV-B.*

An overview of the entire closed-loop system is depicted in Fig. 2

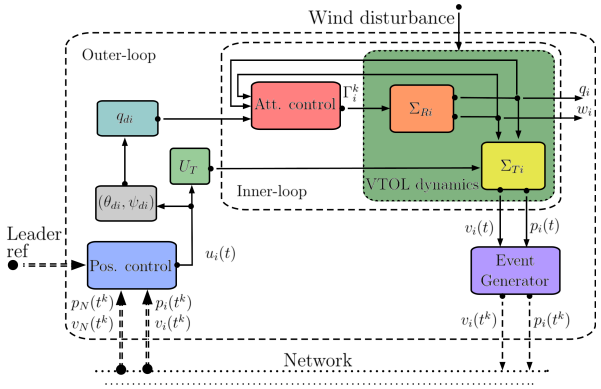

Figure 2: Block diagram of the system.

V. Numerical Simulations

The current section presents the numerical simulation results to validate the proposed control strategy of a group of five VTOL aerial vehicles within realistic aerodynamic conditions.

A. Aerodynamic Simulations

In order to compute the aerodynamic parameters of the aerial vehicles, which correspond to AR drone 2.0 models from PARROT®, the Ansys Fluent® software was used.

The scenario considered for the simulation aims to present the flight of the aerial vehicle in hover. Then, a wind profile coming from different directions and at different speeds is exerted on the drone's airframe. The simulation study allows to determine such forces in function of velocity, the AoA α and the sideslip angle β, see Fig. 3.

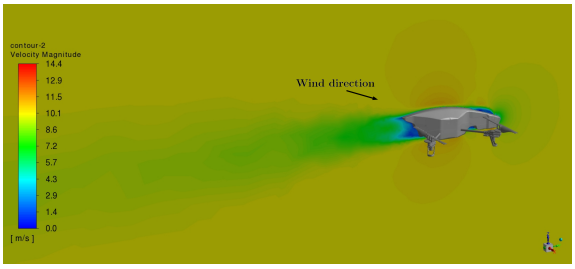

Figure 3: Layout quadcopter wind tunnel simulation considering horizontal wind vector.

B. Simulation Scenario

The set of simulations to assess the proposed control strategy were performed using the Matlab/Simulink® environment.

The simulation model features the parameters depicted in Table I for each VTOL vehicle. Besides, for the case of study presented in this work, five aerial vehicles are considered ($N = 5$). A virtual leader, ($N = 0$), shares to the neighbors its information related to position or trajectory. The communication topology that is used for information exchange between the agents is shown in Fig. 4, and has a directed configuration.

System	Description	Value	Units
Quadcopter	Mass (m)	650	g
	Distance (d)	20	cm
	Inertial moment x (J_ϕ)	0.0075	$Kg \cdot m^2$
	Inertial moment y (J_θ)	0.0075	$Kg \cdot m^2$
	Inertial moment z (J_ψ)	0.013	$Kg \cdot m^2$

Table I: Physical parameters for the VTOL vehicle

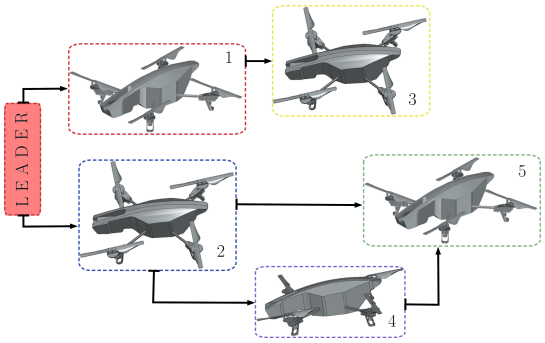

Figure 4: Multi-VTOL system and communication flow.

The corresponding matrices associated with the communication flow between vehicles are given as:

$$\mathcal{A} = \begin{pmatrix} 0 & 0 & 0 & 0 & 0 \\ 0 & 0 & 0 & 0 & 0 \\ 1 & 0 & 0 & 0 & 0 \\ 0 & 1 & 0 & 0 & 0 \\ 0 & 1 & 0 & 1 & 0 \end{pmatrix}, \mathcal{B} = \begin{pmatrix} 1 & 0 & 0 & 0 & 0 \\ 0 & 1 & 0 & 0 & 0 \\ 0 & 0 & 0 & 0 & 0 \\ 0 & 0 & 0 & 0 & 0 \\ 0 & 0 & 0 & 0 & 0 \end{pmatrix} \tag{58}$$

$$\mathcal{D} = \begin{pmatrix} 0 & 0 & 0 & 0 & 0 \\ 0 & 0 & 0 & 0 & 0 \\ 0 & 0 & 1 & 0 & 0 \\ 0 & 0 & 0 & 1 & 0 \\ 0 & 0 & 0 & 0 & 2 \end{pmatrix}, \mathcal{L} = \begin{pmatrix} 0 & 0 & 0 & 0 & 0 \\ 0 & 0 & 0 & 0 & 0 \\ -1 & 0 & 1 & 0 & 0 \\ 0 & -1 & 0 & 1 & 0 \\ 0 & -1 & 0 & -1 & 2 \end{pmatrix} \tag{59}$$

$$\mathcal{H} = \begin{pmatrix} 1 & 0 & 0 & 0 & 0 \\ 0 & 1 & 0 & 0 & 0 \\ -1 & 0 & 1 & 0 & 0 \\ 0 & -1 & 0 & 1 & 0 \\ 0 & -1 & 0 & -1 & 2 \end{pmatrix} \tag{60}$$

The eigenvalues of the matrix $\mathcal{H}$ are 1, 1, 1, 1, 2. Since none of the eigenvalues is 0, then the matrix $\mathcal{H}$ has full rank and there exists at least one spanning tree in the topology.

The control law and trigger mechanism parameters used for the simulation can be found in Table II . Finally, for the

Description	Parameter	Value
Position controller	$\lambda_{ix,iy}$	2.5
	λ_{iz}	1.6
	$K_{six,siy}$	1
	K_{siz}	3
	$\rho_{ix,iy}$	0.8
	ρ_{iz}	0.1
Trigger mechanism	ν_{1i}	1
	ν_{2i}	1
	$\delta_{xi,yi}$	0.01
	δ_{zi}	0.05

Table II: Numerical values for control laws and event function

simulations, two scenarios were considered and are detailed as follows:

1) First Scenario: The consensus of a group of multi-rotor aerial vehicles under unknown disturbances coming from windy conditions. First, the multi-robot system is initialized with the conditions given in the Table III. Then, the vehicles

VTOL MAS	Orientation $^\circ$ $(\phi_i, \theta_i, \psi_i)$	Position m $(p_{x_i}, p_{y_i}, p_{z_i})$
1	(1, -2, 5)	(-1.2, 0.15, 0.01)
2	(2, 3, 1)	(0.1, 1, 0.01)
3	(2, 2, -4)	(1, 0.05, 0.01)
4	(-2, 1, -6)	(0.5, -1, 0.01)
5	(-2, 1, 3)	(-1, 0.8, 0.01)

Table III: Initial conditions for the vehicles

performs consensus with the virtual leader to a position given by $\boldsymbol{p}_0 = (0, 0, 2)^T$m. Once the system is stabilized ($t = 15$s), the virtual leader performs a trajectory described as $\boldsymbol{p}_0 = (2\sin(2\pi t/25), 2\cos(2\pi t/25), 3)^T$m. At $t = 20$s a wind profile, described by Fig. 5a is induced to analyse the performance of the system. The simulation runs for 90s.

2) Second Scenario: The formation control of the multi-agent system under unknown disturbances produced by windy conditions. The initial conditions are the same as in the first scenario, however the multi-robot system performs formation control, where the positions of the agents are intended to form a trapeze over the $x - y$ plane, with the following desired inter-agent distances with respect to the leader: $\boldsymbol{\mu}_1 = (-1, 0, 0)^T$, $\boldsymbol{\mu}_2 = (0, 0, 0)^T$, $\boldsymbol{\mu}_3 = (1, 0, 0)^T$, $\boldsymbol{\mu}_4 = (0.5, 0.9, 0)^T$, $\boldsymbol{\mu}_5 = (-0.5, -0.9, 0)^T$. The set of VTOL's take off and perform formation control to a position given by $\boldsymbol{p}_0 = (0, 0, 2)^T$m. Then, at $t = 15$s a trajectory-tracking is executed and described by $\boldsymbol{p}_0 = \left(\frac{7}{3-\cos(\frac{2t}{25})}\cos(\frac{t}{25}), \frac{7}{3-\cos(\frac{2t}{25})}\frac{\sin(\frac{2t}{25})}{2}, \sin(\frac{2\pi t}{40}) + 4\right)^T$m. At $t = 20$s, a wind profile is generated in order to analyze the performance of the proposed control law. The simulation runs for 250s. A video of this scenario is accessible through the following link: https://www.dropbox.com/s/paahosbuoa0hcu6/event_sliding_2022.mp4?dl=0

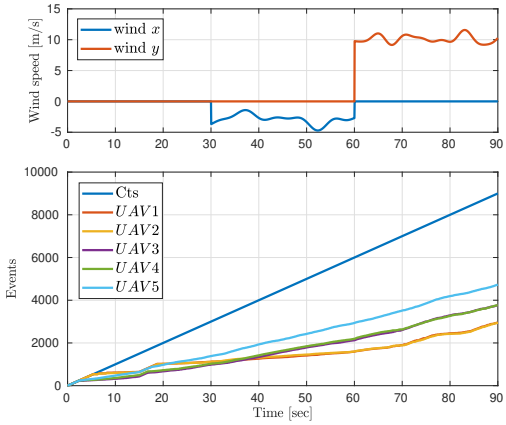

Figure 5: Wind profile and Evolution of the events vs. continuous-time.

C. Simulation Results and Discussion

1) First Scenario: Fig. 5 depicts the wind model profile acting on the system as well as the evolution of the events during the consensus. The behavior of the wind allows us to observe that when its direction and intensity changes, the triggering of events adapts to ensure convergence to the leader. In addition to the behavior of the event mechanism, Figure 5b shows a comparison to a periodic case communication system, where a sampling rate of 0.01s is considered. Then, for the 90s simulation, 9,000 events are produced for the periodic system against the 4,923 of the vehicle that recorded the most events with the proposed strategy, representing a 54% reduction in transmissions and control updates. Table V shows the number of events triggered during the simulation.

Fig. 6 shows the UAVs trajectories and linear velocities during the consensus for each axe. It is shown that practical convergence to the leader in terms of position and velocity is ensured. The good performance of the closed-loop system using the proposed strategy is confirmed through the Table IV, which shows the norm of the errors for every vehicle in the group. It is worth to mention that the norm is computed from the moment the wind is generated ($t = 30$s), showing that the effect of the disturbances is reduced.

$\|e\|$ m	UAV_1	UAV_2	UAV_3	UAV_4	UAV_5
$\|e_x\|$	0.048	0.048	0.053	0.054	0.056
$\|e_y\|$	0.085	0.082	0.073	0.077	0.083
$\|e_z\|$	0.047	0.048	0.086	0.088	0.091

Table IV: Norm of the errors for every vehicle during the consensus

The behavior of the sliding manifolds and the control signals for the different vehicles during the simulation are presented in Fig. 7. Fig. 7a show that for time instants between $[t^k, t^{k+1})$ the state variables show a tendency to deviate from the sliding manifold, but remain bounded within a band near to it. The performance of the event-triggered control law is presented

in Fig. 7b. The time interval between $(10-12)$s is zoomed to illustrate when the control law keeps the last value until the next event is triggered, allowing a reduction in the control solicitation. We can notice that from time $t = 60$s, with average static wind speed $v^s_{\omega_y} = 10$m/s, the adaptive term of the proposed strategy compensates for the unknown static force and consensus for position and velocity are reached again.

2) Second Scenario: Fig. 8 depicts, as in the previous scenario, the wind profile causing unknown disturbances to the system as well as the total of events triggered during the formation control simulation. A comparison to a periodic system is equally performed, and by running the simulation for 250s, $25,000$ events are produced for the periodic case, against the maximum registered with our proposal ($12,060$ events), representing a 48% of reduction in control updates. Table V presents the number of updates when using the event-based control law studied in this work.

The behavior of the multi-VTOL system during the formation on the planar space is presented in Fig. 9a. It shows explicitly the reaction of the system to the changes of the wind directions and intensities. Finally, the $3D$ trajectory tracking performed by the group of aerial vehicles is depicted in Fig. 9b, where some positions are highlighted to show how the control law keeps the formation during the trajectory-following under the external disturbances.

Updates	UAV_1	UAV_2	UAV_3	UAV_4	UAV_5
Scenario 1	2933	2944	3767	3857	4923
Scenario 2	6525	6533	9155	9350	12060

Table V: Control updates for consensus and formation with control law (37)

VI. Conclusions and Perspectives

The actual paper addressed the robust event-based consensus problem and formation control of a group of VTOL-UAVs subject to close-to-reality wind-born disturbances. The dynamic model of the MAS is extended to take into account aerodynamic effects for which a distributed and adaptive event-based sliding mode-control law is synthesized. Merging the inherent robustness furnished by the SMC with the benefits of an event-based scheme, stable closed-loop behavior and low-power computation are achieved. Due to the underactuated nature of the quadrotors, the corresponding motion is based on a two-level (inner-outer loop) control scheme. The performance of the proposed event-triggered MAS control strategy is assessed through Lyapunov-based stability analysis as well as an extensive numerical stage. The simulation results witness the tolerance to unknown-but-bounded disturbances while fulfilling the consensus objective considering an event-triggered control law.

Forthcoming research includes the real-time implementation of the proposed strategy. In addition, the usage of event-triggered control techniques within interactive scenarios, as MAS-based cargo transport or collective manipulation will be investigated.

References

[1] G. S. Seyboth, D. V. Dimarogonas, and K. H. Johansson, "Event-based broadcasting for multi-agent average consensus," *Automatica*, vol. 49, no. 1, pp. 245–252, 2013.

[2] H. Yan, Y. Shen, H. Zhang, and H. Shi, "Decentralized event-triggered consensus control for second-order multi-agent systems," *Neurocomputing*, vol. 133, pp. 18–24, 2014.

[3] C. Nowzari and J. Cortés, "Team-triggered coordination for real-time control of networked cyber-physical systems," *IEEE Transactions on Automatic Control*, vol. 61, no. 1, pp. 34–47, 2015.

[4] D. Yang, W. Ren, X. Liu, and W. Chen, "Decentralized event-triggered consensus for linear multi-agent systems under general directed graphs," *Automatica*, vol. 69, pp. 242–249, 2016.

[5] H. Meng, H.-T. Zhang, Z. Wang, and G. Chen, "Event-triggered control for semiglobal robust consensus of a class of nonlinear uncertain multiagent systems," *IEEE Transactions on Automatic Control*, vol. 65, no. 4, pp. 1683–1690, 2019.

[6] D. Ye, M.-M. Chen, and H.-J. Yang, "Distributed adaptive event-triggered fault-tolerant consensus of multiagent systems with general linear dynamics," *IEEE transactions on cybernetics*, vol. 49, no. 3, pp. 757–767, 2018.

[7] L. Rong and J. Wang, "Fully distributed event-based adaptive control for consensus disturbance rejection," in *2019 Chinese Control Conference (CCC)*. IEEE, 2019, pp. 5972–5977.

[8] J. J. Castillo-Zamora, K. A. Camarillo-GóMez, G. I. PéRez-Soto, and J. RodríGuez-ReséNdiz, "Comparison of pd, pid and sliding-mode position controllers for v–tail quadcopter stability," *IEEE Access*, vol. 6, pp. 38 086–38 096, 2018.

[9] D. Yao, H. Li, R. Lu, and Y. Shi, "Distributed sliding-mode tracking control of second-order nonlinear multiagent systems: an event-triggered approach," *IEEE transactions on cybernetics*, vol. 50, no. 9, pp. 3892–3902, 2020.

[10] A. Sinha and R. K. Mishra, "Consensus in first order nonlinear heterogeneous multi-agent systems with event-based sliding mode control," *International Journal of Control*, vol. 93, no. 4, pp. 858–871, 2020.

[11] R. K. Mishra and A. Sinha, "Event-triggered sliding mode based consensus tracking in second order heterogeneous nonlinear multi-agent systems," *European Journal of Control*, vol. 45, pp. 30–44, 2019.

[12] C. Santos, F. Espinosa, M. Martinez-Rey, D. Gualda, and C. Losada, "Self-triggered formation control of nonholonomic robots," *Sensors*, vol. 19, no. 12, p. 2689, 2019.

[13] C. Dong, M. Ma, Q. Wang, and S. Ma, "Event-based formation control of multiple quadrotors on so (3)," *Mathematical Problems in Engineering*, vol. 2018, 2018.

[14] J. Guerrero-Castellanos, A. Vega-Alonzo, S. Durand, N. Marchand, V. R. Gonzalez-Diaz, J. Castañeda-Camacho, and W. F. Guerrero-Sánchez, "Leader-following consensus and formation control of vtol-uavs with event-triggered communications," *Sensors*, vol. 19, no. 24, p. 5498, 2019.

[15] Z. Cai, H. Zhou, J. Zhao, K. Wu, and Y. Wang, "Formation control of multiple unmanned aerial vehicles by event-triggered distributed model predictive control," *IEEE Access*, vol. 6, pp. 55 614–55 627, 2018.

[16] J. Alvarez-Muñoz, J. Chevalier, J. J. Castillo-Zamora, and J. Escareno, "Distributed event-based sliding-mode consensus control in dynamic formation for vtol-uavs," in *2021 International Conference on Unmanned Aircraft Systems (ICUAS)*. IEEE, 2021, pp. 1364–1373.

[17] B. Bollobás and B. Bollobas, *Modern graph theory*. Springer Science & Business Media, 1998, vol. 184.

[18] N. Deo, *Graph theory with applications to engineering and computer science*. Courier Dover Publications, 2017.

[19] F. R. Chung and F. C. Graham, *Spectral graph theory*. American Mathematical Soc., 1997, no. 92.

[20] J. L. Gross and J. Yellen, *Handbook of graph theory*. CRC press, 2003.

[21] S. Waslander and C. Wang, "Wind disturbance estimation and rejection for quadrotor position control," in *AIAA Infotech@ Aerospace conference and AIAA unmanned... Unlimited conference*, 2009, p. 1983.

[22] B. Ahmed and F. Kendoul, "Flight control of a small helicopter in unknown wind conditions," in *49th IEEE Conference on Decision and Control (CDC)*. IEEE, 2010, pp. 3536–3541.

[23] J. F. Guerrero-Castellanos, N. Marchand, A. Hably, S. Lesecq, and J. Delamare, "Bounded attitude control of rigid bodies: Real-time experimentation to a quadrotor mini-helicopter," *Control Engineering Practice*, vol. 19, no. 8, pp. 790–797, 2011.

[24] L. Derafa, A. Benallegue, and L. Fridman, "Super twisting control algorithm for the attitude tracking of a four rotors uav," *Journal of the Franklin Institute*, vol. 349, no. 2, pp. 685–699, 2012.

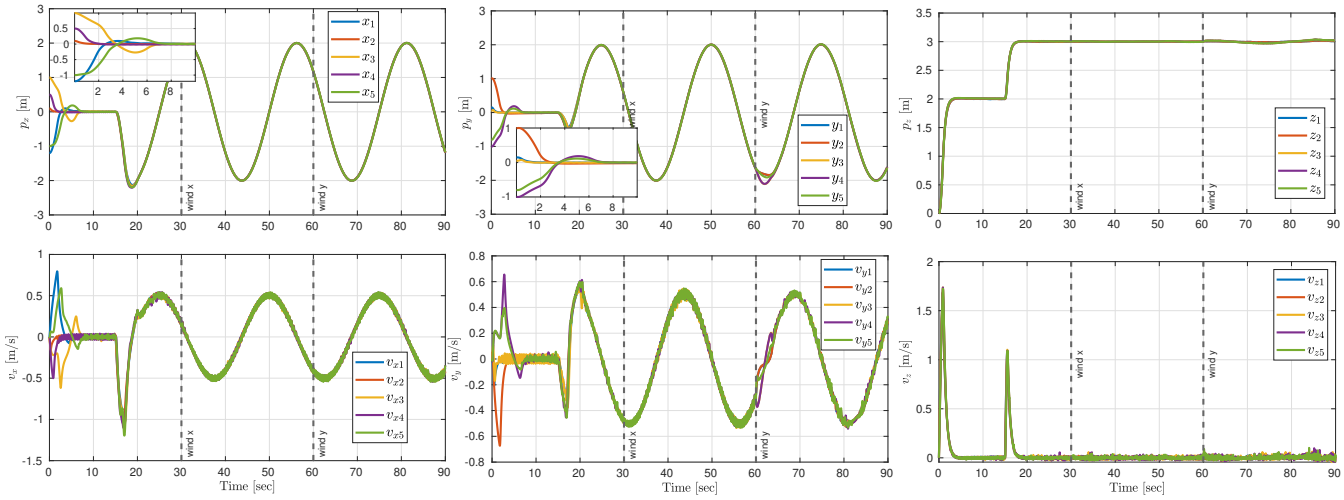

Figure 6: Linear positions and velocities of the aerial vehicles during the consensus.

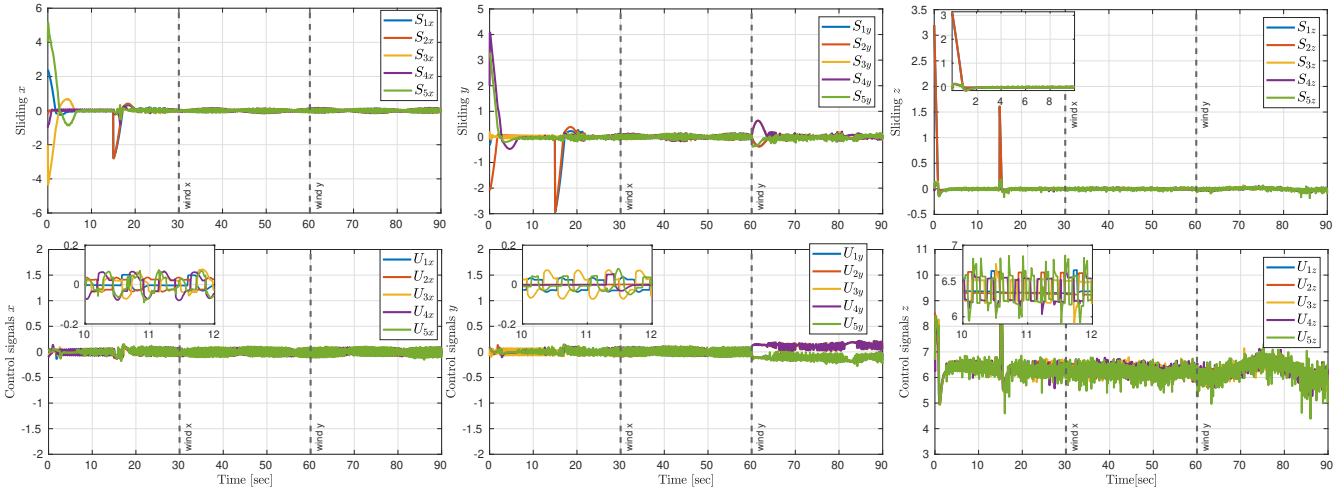

Figure 7: Sliding surface variables and Control inputs performance.

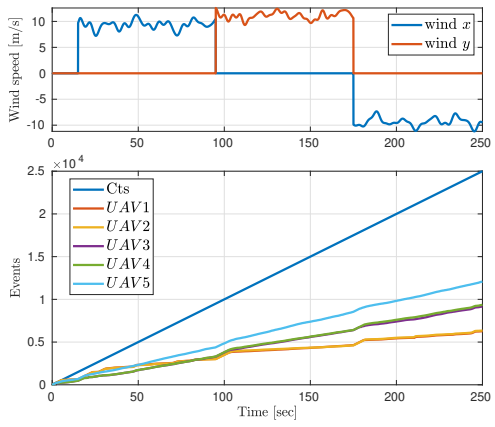

Figure 8: (Top) Wind profile. (Bottom) Evolution of the events vs. continuous-time during the formation.

[25] A. Polyakov and A. Poznyak, "Reaching time estimation for "super-twisting" second order sliding mode controller via lyapunov function designing," *IEEE Transactions on Automatic Control*, vol. 54, no. 8, pp. 1951–1955, 2009.

[26] J. Escareño, S. Salazar, H. Romero, and R. Lozano, "Trajectory control of a quadrotor subject to 2d wind disturbances," *Journal of Intelligent & Robotic Systems*, vol. 70, no. 1, pp. 51–63, 2013.

[27] H. K. Khalil, "Nonlinear systems third edition," *Patience Hall*, vol. 115, 2002.

J. U. Alvarez-Muñoz received the M.Sc.in 2012 in Electronics, from the Autonomous University of Puebla, Mexico and the Ph.D. degree in 2017 in Automatic Control from GIPSA-Lab from the University of Grenoble (UGA), France. From January 2018 to March 2019, he has held a Post-Doctoral fellowship position at the Institut Polytechnique des Sciences Avancées (IPSA) at Ivry-sur-Seine, France. Currently, he holds a research position at "EXTIA", in the robotics department in Paris, France. His current general research interests are focused on the modeling and control of convertible and interactive drones and multi-agent control systems in the field of aerial robotics.

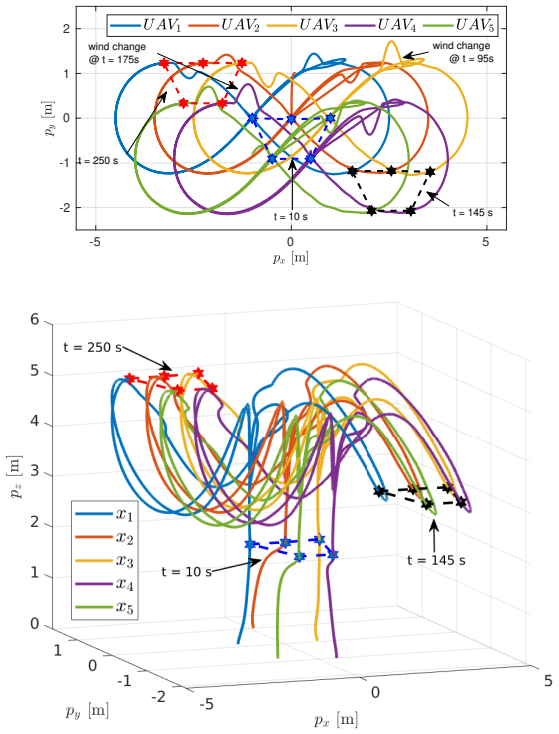

Figure 9: (Top) Planar positions of the vehicles and (Bottom) 3D positions of the vehicles during the formation.

J. Escareno received a Ph.D. (2008) in Automatic Control from the HEUDIASYC laboratory of the University of Technology of Compiegne (UTC) , France. From 2008 to 2010, he held a Post-Doctoral fellowship at the "Unité Mixte de Internationale du CNRS - UMI 3175". He was a CNRS project researcher at the UTC, from 2010 to 2012. In 2012, he has held a four-month stay as a visiting scientist at the French Nuclear Energy Commission (CEA). He served, from 2012 to 2013, as a Post-Doctoral Research Associate at the department of "Automatique et Systèmes Micro-Mécatroniques" (AS2M) at FEMTO-ST UMR CNRS 6174, France. From 2014-2018, he held an associate professor position at the "Institut Polytechnique des Sciences Avancées" at Ivry-sur-Seine, France. Since 2018, he is associate professor at XLim CNRS Research Institute and ENSIL-ENSCI Engineering School at University of Limoges. His current research encompasses nonlinear control of multi-agent systems, hybdrid and interactive robotic systems and autonomous robust navigation.

J. Chevalier received the M.Sc in 2016 in Mechatronics engineering from the University Blaise Pascal. From 2016 to 2018 He has held a mechanical engineering position at SoftBank Robotics. Currently, he holds a R&D robotics engineer position at "EXTIA", in the robotics department.

S. Daix received the M.Sc in 2007 in modeling and simulation of physical systems. He continued with a Technological Research Diploma at the Atomic Energy Commission for 18 months. Since the beginning of 2016, he has been the technical referent within the CFD and Thermal design office of PSA. Its main mission is the development of the digital sector of the underhood environment (Fluent and Taitherm) taking into account the aeraulics and the modeling of heat exchanges (conduction, convection and radiation).

O. Labanni-Igbida received the Eng. and PhD Degrees in robotics from the ENSMM-University of Franche-Comte, and the Habilitation Degree in vision and robotics from the University of Picardie Jules Verne, France. Since 2013, she has been Full Professor with XLim CNRS Institute of Research and ENSIL-ENSCI Engineering School at University of Limoges. She is the Head of the Mechatronics Department at ENSIL-ENSCI Engineering School and supervises the Robotics and Mechatronics research group at the XLim institute. Her main research interests are in the field of robotics, including enactive perception and control, omnidirectional catadioptric vision, cooperative robotics, and localization and navigation of autonomous systems.